Article

Journal of the Brazilian Chemical Society

https://dx.doi.org/10.21577/0103-5053.20240106

J. Braz. Chem. Soc. **2024**, *35*, 12, e-20240106, 1-7

Tailoring Charge Carriers through Solid-State Mechanochemical Synthesis Bismuth Nanoparticles Directly onto $BiVO_4$ Surface

Leandro A. Faustino,[*,a] *Ismael P. L. Xavier,*[a] *Paulo F. M. de Oliveira*[a] *and Susana I. Cordoba de Torresi*[*,a]

[a]*Instituto de Química, Universidade de São Paulo, Av. Prof. Lineu Prestes 748, 05360-050 São Paulo-SP, Brazil*

Metallic nanoparticles remain the focus of diverse studies across various fields due to their exceptional properties and applications in biology, sensing, energy, and (electro)catalysis. Typical syntheses of metallic nanoparticles are solution-based and require the use of stabilizing agents. Although these surface agents prevent agglomeration, they also hinder access to active sites on the nanoparticle surface. A promising alternative is mechanochemical synthesis, offering a solvent and surfactant-free approach, which yields uniform nanoparticles with clean surfaces. Here, we employ ball milling as a mechanochemical method to prepare metallic bismuth nanoparticles in a single step, using $BiVO_4$ semiconductor both as a bismuth source and a support. Our results demonstrate that, in addition to the formation of nanoparticles by the partial reduction of $BiVO_4$, there is an increase in charge carriers in the semiconductor structure as probed by electrochemical experiments. The final properties of Bi@$BiVO_4$ material make it a relevant candidate for (electro)catalysis.

Keywords: bismuth nanoparticles, semiconductors, mechanochemistry, charge carriers

Introduction

Nanomaterials, particularly metallic nanoparticles (NPs), continue to gain attention due to their properties and consequent applications in various fields such as biology, energy devices and catalysis, among others.[1-6] The small size of the NPs (1-100 nm) reflects in unique properties which include a high surface area, electrical conductivity, and physical chemical properties like modified optical, mechanical, and thermal stability.[7] Furthermore, the metal NPs have photoinduced properties due to the localized surface plasmon resonance (LSPR), in which, when the NPs are light-irradiated by an appropriated wavelength, typical in the UV-Vis range, the electromagnetic field induces the electron oscillation over the NPs surface, resulting in dipoles. As a result, local effects are observed, like increases in the local temperature, generation of hot carriers and near field enhancement.[8]

Different ways to synthesize metal NPs have been studied for decades, such as electrodeposition, sputtering and solution-based methods, which include chemical reduction, sol-gel, and hydrothermal methods.[9] As the properties of the NPs are strongly affected by the shape and size, the selected method of synthesis can be very important, since the interaction of the metal ions and reducing agents, stabilizing agent, precursor and solvents can change the final structure of the NPs.

The bottom-up mechanochemical synthesis of metal NPs has gained more attention in the last years because it is considered a green and scalable alternative route to produce metallic NPs.[10,11] In terms of the synthesis of NPs, the attention given to mechanochemical means is attributed to the fact that it does not require the use of solvents or stabilizing agents, producing uniform NPs with a clean surface allowing to explore their properties for different applications.[12] In addition, the synthesis of NPs over solid supports can be performed in one-pot by the chemical reduction of the metal precursor, followed by the nucleation and growth on the surface of the support.

In the present work, we explore the bottom-up mechanochemical route using ball milling to synthesize metallic bismuth (Bi) NPs by chemical reduction. $BiVO_4$ served as both support and Bi source, resulting in Bi@$BiVO_4$ materials with modified electrochemical and optical properties. The final materials were structurally characterized by powder X-ray diffraction (PXRD), UV-Vis diffuse reflectance spectroscopy (UV-Vis DRS) and

*e-mail: leandrofaustino@usp.br; storresi@iq.usp.br
Editor handled this article: André Galembeck (Guest)
This paper is dedicated to our colleague, friend, excellent scientist and inspiring professor Oswaldo Alves. His legacy will always remain in the Brazilian chemical community.

transmission electron microscopy (TEM). Electrochemical studies were also conducted and demonstrated the effect of the amount of the reducing agent used for BiNPs formation on the density of the charge carriers.

Experimental

Materials

All solvents were high-performance liquid chromatography (HPLC) grade. $Bi(NO_3)_3.5H_2O$ (99%), NH_4VO_3 (98%), $AgNO_3$ (99%), and $NaBH_4$ (98%) were purchased from Aldrich (St. Louis, USA). Milli-Q water was used throughout the experiments.

Synthesis of $BiVO_4$

Initially, the $BiVO_4$ was synthesized following similar procedures previously reported in the literature by a wet route.[13,14] Typically, 3.0 mmol NH_4VO_3 and 3.0 mmol $Bi(NO_3)_3.5H_2O$ were dissolved in 12 mL of hot water and 12 mL of ethyleneglicol, respectively. Afterwards, the NH_4VO_4 solution was slowly dropwised in $Bi(NO_3)_3.5H_2O$ solution and vigorously stirred for 2 h. Then, the mixture was kept in a furnace at 90 ºC overnight resulting in a gel, which was further calcinated at 550 ºC for 120 min (3 ºC min^{-1}) to form $BiVO_4$.

Synthesis of Bi@$BiVO_4$

The Bi@$BiVO_4$ structures were synthesized through a mechanochemical route. In a poly(methyl methacrylate) (PMMA) jar, the pristine $BiVO_4$ and the reducing agent $NaBH_4$ were milled in different m/m ratios in a vibratory ball mill (Pulverissette 23, St. Louis, USA) with a single zirconia ball (2.8 g, diameter ø = 10 mm) for 30 min at 50 Hz. The final powder was recovered and washed several times with water, ethanol, and acetone to remove any residual and dried under vacuum. The ratios chosen were 1, 2.5, 5 and 10% of $NaBH_4$ in relation to the $BiVO_4$ (m/m) to give 1-Bi@$BiVO_4$, 2.5-Bi@$BiVO_4$, 5-Bi@$BiVO_4$ and 10-Bi@$BiVO_4$, respectively. In addition, the pristine $BiVO_4$ was also milled in the absence of a reducing agent, $NaBH_4$, at the same conditions previously described giving M@$BiVO_4$.

Characterization

Powder X-ray diffraction (PXRD) patterns were recorded in Shimadzu 7.000 Maxima diffractometer (Kyoto, Japan) with Cu Kα radiation (λ Cu Kα = 1.5418 Å for combined $K\alpha_1$ and $K\alpha_2$) in a Bragg-Brentano geometry. The transmission electron microscopy (TEM) and high-resolution TEM (HRTEM) images were recorded in JEOL JEM 2100 (Peabody, USA) operated at 200 kV. The samples were prepared by drop casting using 5 µL of the materials in isopropanol/water (1:1). For the TEM and HRTEM images the samples were placed in copper grids. The UV-Vis diffuse reflectance spectra (UV-Vis DRS) of the solid samples were recorded in a Shimadzu UV-2600 UV-Vis spectrophotometer (Kyoto, Japan).

Rietveld refinement

Microstructure analysis and Rietveld refinement of monoclinic $BiVO_4$ and Bi hexagonal phases were conducted using Fullprof Suite software.[15] The positions of diffraction peaks were calibrated using high-purity silicon as an external standard under identical experimental conditions as the samples, i.e., with a scanning step of 0.3° (2θ) and a range of 10 to 80°. Rietveld refinement quality was assessed using standard agreement indices, including the residual factor (Rp), weighted residual factor (Rwp), and the goodness-of-fit factor (χ^2). Additionally, microstructure assessment was performed using the Thomson-Cox-Hastings (TCH) method. This approach utilizes Debye-Scherrer geometry and incorporates variations in Gaussian and Lorentzian half-widths to accurately represent experimental data.

Electrochemical measurements

All the electrochemical experiments were carried out in a Autolab PGSTAT 302N (Uterecht, Netherlands) coupled with three electrodes cell and using 0.2 mol L^{-1} $KHCO_3$ as supporting electrolyte and glassy carbon (area = 0.04 cm^2) as working electrode. The glassy carbon electrodes were also cleaned electrochemically in H_2SO_4 0.5 mol L^{-1} solution. The materials were deposited over the glassy carbon electrodes according to the following steps: 10.3 mg of the materials were dispersed in 700 µL of ethanol, 270 µL of water and 30 µL of Nafion solution 0.05%. The dispersion was sonicated for 1 h and then 7 µL were loaded over the electrode surface. $Ag/AgCl/Cl^-_{(sat)}$ electrode was used as reference and a platinum wire as a counter-electrode. All the potentials were converted to reversible hydrogen electrode (RHE) through the following equation $E_{(V\ vs\ RHE)} = E_{(V\ vs\ Ag/AgCl/Cl^-_{(sat)})} + 0.0591 \times pH + 0.197$ (pH = 8.9 in Ar in 0.2 mol L^{-1} $KHCO_3$) and carried out at room temperature.

The extension of charge carriers on the final materials produced by the milling process in the presence of a $NaBH_4$

as reducing agent was estimated by Mott-Schottky plots analysis based on the changes in the density of the charge carriers. Then, impedance experiments were carried out in the capacitive potential range and the plots were constructed by the following equation.[16]

$$\frac{1}{C^2} = \frac{2}{\varepsilon\varepsilon_0 A^2 e N_d}\left(V - V_{fb} - \frac{k_B T}{e}\right) \quad (1)$$

where C is the differential capacitance, ε dielectric constant of the semiconductor (86 = $BiVO_4$),[17] ε_0 vacuum electric permittivity, A area, *e* elemental charge, N_d density of the charge carriers, V applied potential, V_{fb} flatband potential, k_B is the Boltzmann constant and T is the temperature.

Results and Discussion

The resulting Bi@$BiVO_4$ materials prepared mechanochemically were initially characterized by PXRD, Figure 1. The Bragg reflections observed for the pristine $BiVO_4$ are consistent with the PXRD pattern of monoclinic $BiVO_4$ (JCPDS 98-010-0602). The milled material in the absence of $NaBH_4$, M@$BiVO_4$, also exhibits the same reflections observed for the pristine material, indicating no phase transition as a result of mechanical milling. For the materials milled in the presence of a reducing agent, $NaBH_4$, the reflections relative to the $BiVO_4$ are still maintained. However, the peak intensities are decreased probably due to the loss of crystallinity, resulted from the mechanical stress in the material structure, and the partial disorder caused by the inclusion of $NaBH_4$ in the media. In addition, the PXRD patterns of the materials 5-Bi@$BiVO_4$ and 10-Bi@$BiVO_4$ presents a new reflection at 2θ = 27º (012), which matches with the metallic bismuth in a hexagonal crystalline structure (JCPDS 98-005-3797). Further less intense reflections at 2θ = 38º, 48º, 62º and 64º are also consistent with the metallic hexagonal phase of bismuth. The PXRD results clearly demonstrate that the formation of metallic bismuth is a result of the partial reduction of $BiVO_4$ by $NaBH_4$ resulting in Bi^0 over a $BiVO_4$ stressed structure. In fact, the formation of metallic bismuth starting from $BiVO_4$ have already been reported in the literature,[14,18] however, the authors reported the synthesis based on solution and temperature dependence. In our solid state mechanochemical approach, the use of solvents or higher temperatures are not necessary, producing the same results in Bi NPs in a well distribution.

Rietveld refinement was carried out for the following samples, 5-Bi@$BiVO_4$ and 10-Bi@$BiVO_4$. The Rietveld refinement revealed that the fraction (in percentage) of metallic bismuth formed during the mechanochemical synthesis are 3.08 and 3.79% for 5-Bi@$BiVO_4$ and 10-Bi@$BiVO_4$ respectively (see Table S1 in Supplementary Information (SI) section). The data revealed that the fraction of metallic bismuth does not increase in the same step as the amount of $NaBH_4$ is added in the synthesis.

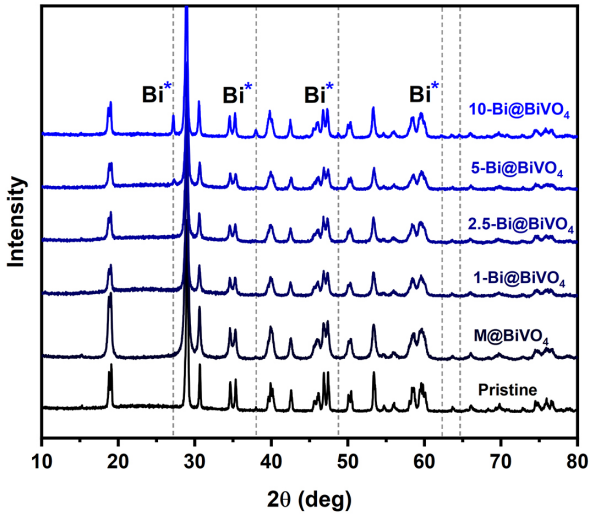

Figure 1. (a) PXRD patterns of (from bottom to top) pristine $BiVO_4$, M@$BiVO_4$, 1-Bi@$BiVO_4$, 2.5-Bi@$BiVO_4$, 5-Bi@$BiVO_4$ and 10-Bi@$BiVO_4$ materials.

The morphology of the materials was investigated by TEM, Figure 2. The pristine $BiVO_4$ and the M@$BiVO_4$ displayed well-defined lattice with an interplanar distance of 0.584 nm, corresponding to the (020) plane of monoclinic phase of $BiVO_4$, the same phase identified in the PXRD patterns. Regarding the $BiVO_4$ milled in the presence of different amounts of $NaBH_4$, one can easily see a uniform distribution of spherical nanoparticles over the $BiVO_4$ sites (Figures 2c-2f). The size of these nanoparticles ranges around 7 ± 1 nm, with an interplanar distance calculated of d = 0.328, which corresponds to the (012) planes of metallic hexagonal bismuth, also in agreement with the PXRD patterns. Interestingly, different from PXRD patterns of reduced samples, which only displayed the reflections of Bi(0) when higher amounts of $NaBH_4$ (5 and 10%) were added, the TEM images show that already with 1% of the reducing agent, Bi(0) can be formed (Figure 2c). The apparent divergence between PXRD and TEM is most probably due to the low content of Bi(0) when $NaBH_4$ is used below 5 wt.%, which makes it difficult to detect Bi(0) by PXRD in our conditions of acquisition. Additionally, a deep investigation of the size of nanoparticles by TEM images, revealed that in higher concentrations of $NaBH_4$, i.e., 5 and 10%, another family of large Bi NPs are produced along with the small ones, with sizes around 24 nm for 5-Bi@$BiVO_4$ and 50 nm for 10-$BiVO_4$ (see Figures S1 and S2, SI section). This

apparently intriguing result is a consequence of welding/coalesce of smaller NPs quickly formed at the beggining of the reaction, when there is more $NaBH_4$ in the system. Then, the constant action of mechanical energy will induce the coalescence and welding of the small NPs, resulting in another family of particle sizes, in addition of that of 7 nm.[19]

The optical properties of the $BiVO_4$ and $Bi@BiVO_4$ materials were investigated, Figure 3. The UV-Vis DRS for the pristine material presents higher percentual of reflectance between 500-800 nm; for the milled materials $Bi@BiVO_4$, as the amount of $NaBH_4$ increases, the absorption over this range is increased, Figure 3a. In order to investigated the effect associated to it, the band gap of the materials was calculated by Tauc Plot considering the Kubelka-Munk function applied to the UV-Vis DRS of solids (see SI section). The band gap achieved for the pristine $BiVO_4$ is 2.50 eV, which agrees with other reports in the literature for the $BiVO_4$ with values between 2.40 and 2.50 eV.[20,21] The milled materials, however, both in the presence and absence of reducing agent, no significant differences in the band gap energy could be observed, with values close to 2.53 eV. The values achieved reveal that the production of Bi NPs on the $BiVO_4$ surface does not lead to significant changes in the energy of the band gap of the semiconductor. Otherwise, observations in terms of reflectance percentage and changes in the solid color, Figure 3c, were observed suggesting that other effects are related to the changes in the optical properties of $Bi@BiVO_4$ materials. Then, the solids were suspended in acetonitrile and the UV-Vis spectra recorded in the transmission mode, Figure 3b. The pristine and the milled material in the absence of $NaBH_4$ material do not present any bands between 400-800 nm. For the materials milled in the presence of a reducing agent, a band is observed in 460 nm and is related to the plasmon band of bismuth nanoparticles.[22] For the materials milled in the presence of high amounts of $NaBH_4$, i.e., 5 and 10%, a broad band between 500 and 800 nm is observed. The broad band absorption observed for the milled materials with higher amounts of $NaBH_4$ can be a result of a production of large bismuth nanoparticles, as observed by TEM images and

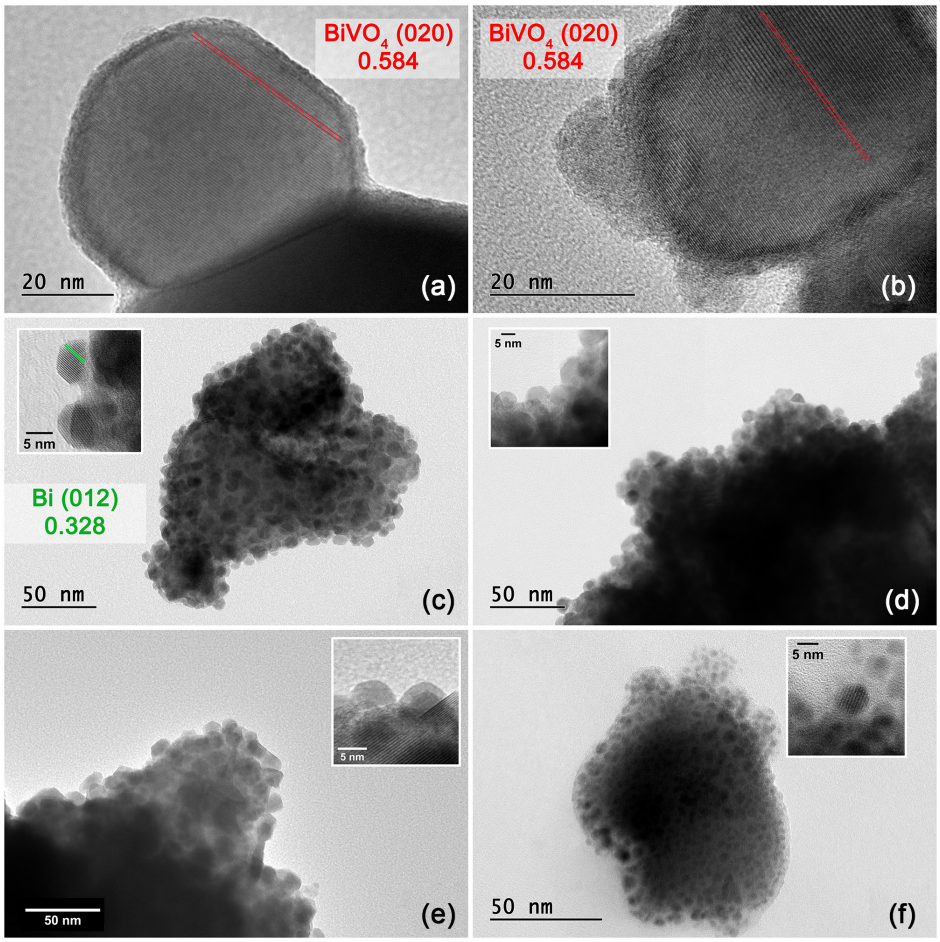

Figure 2. TEM images for (a) the $BiVO_4$, $M@BiVO_4$, 1-$Bi@BiVO_4$, 2.5-$Bi@BiVO_4$, 5-$Bi@BiVO_4$ and 10-$Bi@BiVO_4$ materials. Inset: detail of the size and planes of Bi metallic nanoparticles.

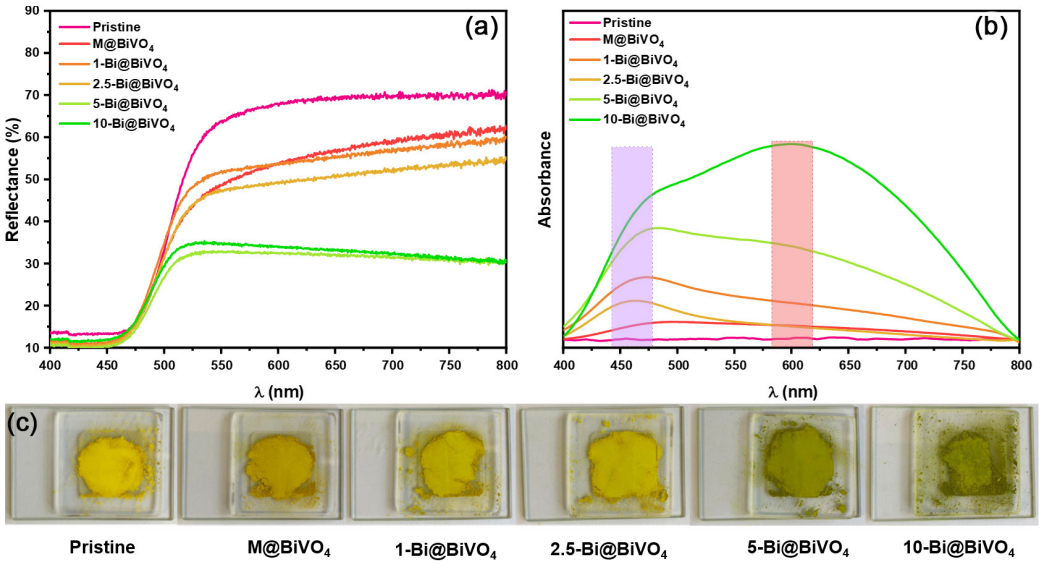

Figure 3. (a) UV-Vis DRS, (b) UV-Vis in transmission mode and (c) color changes of pristine $BiVO_4$, M@$BiVO_4$, 1-Bi@$BiVO_4$, 2.5-Bi@$BiVO_4$, 5-Bi@$BiVO_4$ and 10-Bi@$BiVO_4$ materials.

by the crystallite size obtained by Rietveld refinement. In fact, the plasmon bands of metallic nanoparticles are highly dependent of the shape and size. Some reports in literature[23,24] observed that, as the size of bismuth nanoparticles increase, there is a red-shift in the UV-Vis spectra of bismuth plasmon band.

The milling process in the presence of a reducing agent can result not only in the formation of metallic nanoparticles as reported here, but also in defects in the structure of semiconductors such as oxygen vacancies,[25] that can be valuable for some applications, especially photocatalytic ones.[26] The production of these species directly affects the density of charge carriers. Electrochemical measurements were then used to evaluate and estimate the changes in the density of the charge after the milling process, by employing the Mott-Schottky equation, Figure 4.

The Mott-Schottky analysis was conducted in the capacitive range of potential and exhibits a linear region with a positive slope for all the materials. The positive slope is a typical behavior of n-type semiconductors and can be used to estimate the density of charge carriers (N_d) applying the Mott-Schottky equation.[27] Regarding $BiVO_4$ and M@$BiVO_4$, the estimated N_d values have the same magnitude with values of 6.2×10^{20} and 3.0×10^{20} cm^{-3}, respectively. For the materials milled with 1 and 2.5 wt.% of $NaBH_4$, the N_d values also falls in the same magnitude when compared to the pristine $BiVO_4$ and M@$BiVO_4$ with values of 7.7×10^{20} and 9.7×10^{20} cm^{-3} respectively for 1-Bi@$BiVO_4$ and 2.5-Bi@$BiVO_4$. Despite being of similar order, one can already observe a small increase in the number of charge carriers, when comparing the pristine and the milled systems in the presence of a reducing agent. The difference becomes clearer when higher amounts of reducing agent (5 and 10 wt.% of $NaBH_4$) is employed

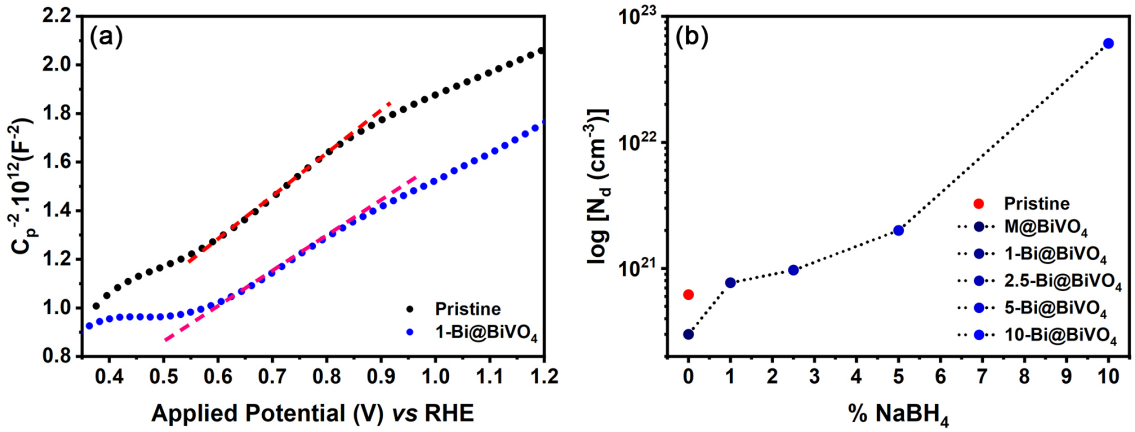

Figure 4. Mott-Schottky plots for (a) $BiVO_4$ pristine and 1-Bi@$BiVO_4$, (b) charge carriers' density obtained for all materials by Mott-Schottky plots at 100 Hz in 0.2 mol L^{-1} $KHCO_3$.

(Figure 4). The density of charge carriers increases significantly in terms of magnitude presenting values of 2.0×10^{21} and 6.1×10^{22} cm^{-3} for 5-Bi@$BiVO_4$ and 10-Bi@$BiVO_4$, respectively. Therefore, concerning the materials milled with the reducing agent, it is possible to observe a trend. The higher the amount of $NaBH_4$, the higher the density of charge carriers, with a more pronounced difference for higher concentrations of reducing agent.

One can attribute the increase of the charge carriers to the reduction of part of Bi^{3+} from $BiVO_4$ into Bi^0 producing metallic Bi NPs. Nonetheless, it is not possible to rule out the possible formation of oxygen vacancies during the milling process in the presence of the reducing agent. There are some reports that observe the formation of oxygen vacancies during the milling process. For instance, oxygen vacancies were formed in CuO structure when milled with Mg as reducing agent, according to Chen *et al*.[28] Another interesting example is related to the chemical reduction of Au^{3+} over MoO_3 in the presence of $NaBH_4$, resulting in the formation of metallic AuNPs over a defective MoO_{3-x} structure.[29] However, when compared to MoO_{3-x} case, for Bi@$BiVO_4$ there is no meaningful change in the band gap.

The increase in the density of charge carriers in the semiconductor structure driven by the formation of NPs and defects through mechanochemistry can be advantageous for the development of materials based on semiconductors. This strategy has potential to be beneficial in different fields, such as catalysis enhanced by localized surface plasmon resonance.

Conclusions

The pristine $BiVO_4$ semiconductor was synthesized through a wet route and submitted to the milling process in different ratios of a reducing agent. In a one-pot synthesis, the mechanochemical approach could generate metallic Bi NPs over $BiVO_4$, without external heating or use of surface agents and solvents. PXRD and TEM confirmed that the milling process induces the formation of metallic Bi nanoparticles well distributed onto $BiVO_4$ surface. Although no significant changes were observed in the band gap of Bi@$BiVO_4$ materials, the changes of color and UV-Vis absorption spectra revealed red-shifted bands in the presence of higher amounts of $NaBH_4$ due to the formation of large Bi NPs. Besides no significant changes in the amount of metallic Bi produced in higher amounts of $NaBH_4$, the electrochemical measurements through Mott-Schottky analysis indicate that the number of charge carriers increases according to the amount of reducing agent used. The mechanochemical synthesis of Bi@$BiVO_4$, displaying both nanoparticles and semiconductor properties, can be used to tune the density of charge carriers for different applications, especially catalytic ones. Furthermore, the mechanochemical synthesis approach can amplify the use of solid-state ball milling for the preparation of multicomponent advanced materials for technological applications.

Supplementary Information

Supplementary data are available free of charge at http://jbcs.sbq.org.br as PDF file.

Acknowledgments

The authors are thankful to Fundação de Amparo à Pesquisa do Estado de São Paulo (FAPESP, 20/15230-5, 21/00675-4, 22/04604-7, 23/01223-5), Conselho Nacional de Desenvolvimento Científico e Tecnológico (303269/2021-9). PFMO also acknowledge FAPESP for funding (FAPESP 2020/14955-6). The authors would also thankfully acknowledge the support of the RCGI-Research Centre for Greenhouse Gas Innovation, hosted by the University of São Paulo (USP) and sponsored by FAPESP and Shell Brasil, and the strategic importance of the support given by ANP (Brazil's National Oil, Natural Gas, and Biofuels Agency) through the R&D levy regulation.

Author Contributions

Leandro A. Faustino was responsible for investigation, methodology, data curation, writing-original draft, review and editing; Ismael P. L. Xavier for investigation, writing-original draft, review and editing; Paulo F. M. de Oliveira for investigation, writing-review and editing; Susana I. Cordoba de Torresi for supervision, writing-review and editing, resources.

References

1. da Silva, R. T. P.; Petri, M. V.; Valencia, E. Y.; Camargo, P. H. C.; de Torresi, S. I. C.; Spira, B.; *Photodiagnosis Photodyn. Ther.* **2020**, *31*, 101908. [Crossref]
2. Durán, N.; Marcato, P. D.; de Conti, R.; Alves, O. L.; Costa, F. T. M.; Brocchi, M.; *J. Braz. Chem. Soc.* **2010**, *21*, 949. [Crossref]
3. Abbasi-Ahd, A.; Shokoufi, N.; Adeleh, S.; Kargosha, K.; *J. Braz. Chem. Soc.* **2017**, *28*, 1843. [Crossref]
4. Stratakis, E.; Kymakis, E.; *Materials Today* **2013**, *16*, 133. [Crossref]

5. Miguel, V. M.; Rodrigues, M. P. S.; Braga, A. H.; de Torresi, S. I. C.; *ACS Appl. Nano Mater.* **2022**, *5*, 2943. [Crossref]
6. Rodrigues, M. P. S.; Dourado, A. H. B.; Cutolo, L. O.; Parreira, L. S.; Alves, T. V.; Slater, T. J. A.; Haigh, S. J.; Camargo, P. H. C.; Cordoba de Torresi, S. I.; *ACS Catal.* **2021**, *11*, 13543. [Crossref]
7. Yaqoob, A. A.; Ahmad, H.; Parveen, T.; Ahmad, A.; Oves, M.; Ismail, I. M. I.; Qari, H. A.; Umar, K.; Mohamad Ibrahim, M. N.; *Front Chem.* **2020**, *8*, 341. [Crossref]
8. Rodrigues, M. P. S.; Dourado, A. H. B.; Sampaio de Oliveira-Filho, A. G.; de Lima Batista, A. P.; Feil, M.; Krischer, K.; Córdoba de Torresi, S. I.; *ACS Catal.* **2023**, *13*, 267. [Crossref]
9. Jamkhande, P. G.; Ghule, N. W.; Bamer, A. H.; Kalaskar, M. G.; *J. Drug Delivery Sci. Technol.* **2019**, *53*, 101174. [Crossref]
10. Baláž, M.; Bedlovičová, Z.; Daneu, N.; Siksa, P.; Sokoli, L.; Tkáčiková, Ľ.; Salayová, A.; Džunda, R.; Kováčová, M.; Bureš, R.; Bujňáková, Z. L.; *Nanomaterials* **2021**, *11*, 1139. [Crossref]
11. de Oliveira, P. F. M.; Torresi, R. M.; Emmerling, F.; Camargo, P. H. C.; *J. Mater. Chem. A* **2020**, *8*, 16114. [Crossref]
12. da Silva, R. T. P.; Córdoba de Torresi, S. I.; de Oliveira, P. F. M.; *Front Chem.* **2022**, *10*, 836597. [Crossref]
13. Yuan, M.; Chen, J.; Bai, Y.; Liu, Z.; Zhang, J.; Zhao, T.; Shi, Q.; Li, S.; Wang, X.; Zhang, G.; *Chem. Sci.* **2021**, *12*, 6048. [Crossref]
14. Yuan, M.; Chen, J.; Bai, Y.; Liu, Z.; Zhang, J.; Zhao, T.; Wang, Q.; Li, S.; He, H.; Zhang, G.; *Angew. Chem., Int. Ed.* **2021**, *60*, 10910. [Crossref]
15. *Fullprof Suite*, v. 5.10; Institut Laue-Langevin, Grenoble, France, 2001.
16. Gelderman, K.; Lee, L.; Donne, S. W.; *J. Chem. Educ.* **2007**, *84*, 685. [Crossref]
17. Ye, K.-H.; Yu, X.; Qiu, Z.; Zhu, Y.; Lu, X.; Zhang, Y.; *RSC Adv.* **2015**, *5*, 34152. [Crossref]
18. de Brito, J. F.; Corradini, P. G.; Zanoni, M. V. B.; Marken, F.; Mascaro, L. H.; *J. Alloys Compd.* **2021**, *851*, 156912. [Crossref]
19. de Oliveira, P. F. M.; Torresi, R. M.; Emmerling, F.; Camargo, P. H. C.; *J. Mater. Chem. A* **2020**, *8*, 16114. [Crossref]
20. Chen, X.; Wu, Y.; Deng, M.; Shen, H.; Ding, J.; Wang, W.; *ACS Omega* **2022**, *7*, 17075. [Crossref]
21. Pingmuang, K.; Chen, J.; Kangwansupamonkon, W.; Wallace, G. G.; Phanichphant, S.; Nattestad, A.; *Sci. Rep.* **2017**, *7*, 8929. [Crossref]
22. Singh, S. P.; Karmakar, B.; *Mater. Chem. Phys.* **2010**, *119*, 355. [Crossref]
23. McMahon, J. M.; Schatz, G. C.; Gray, S. K.; *Phys. Chem. Chem. Phys.* **2013**, *15*, 5415. [Crossref]
24. Wang, Z.; Jiang, C.; Huang, R.; Peng, H.; Tang, X.; *J. Phys. Chem. C* **2014**, *118*, 1155. [Crossref]
25. Zou, W.; Dong, J.; Ji, M.; Wang, B.; Li, Y.; Yin, S.; Li, H.; Xia, J.; *ACS Appl. Nano Mater.* **2023**, *6*, 4309. [Crossref]
26. Hao, L.; Yan, J.; Guan, S.; Cheng, L.; Zhao, Q.; Zhu, Z.; Wang, Y.; Lu, Y.; Liu, J.; *Appl. Surf. Sci.* **2019**, *466*, 490. [Crossref]
27. Hankin, A.; Bedoya-Lora, F. E.; Alexander, J. C.; Regoutz, A.; Kelsall, G. H.; *J. Mater. Chem. A* **2019**, *7*, 26162. [Crossref]
28. Chen, H.; Zhou, S.; Han, Z.; Jiang, Y.; Yu, H.; Zhou, X.; Jiang, R.; Liu, X.; Li, X.; *J. Mater. Chem. A* **2016**, *4*, 17207. [Crossref]
29. Quiroz, J.; de Oliveira, P. F. M.; Shetty, S.; Oropeza, F. E.; de la Peña O'Shea, V. A.; Rodrigues, L. C. V.; de S. Rodrigues, M. P.; Torresi, R. M.; Emmerling, F.; Camargo, P. H. C.; *ACS Sustainable Chem. Eng.* **2021**, *9*, 9750. [Crossref]

Submitted: January 30, 2024
Published online: June 18, 2024